Dipartimento di Elettronica e Informazione e Bioingegneria

Politecnico di Milano

20133 Milano (Italia)
Piazza Leonardo da Vinci, 32
Tel. (39) 02-2399.3400
Fax (39) 02-2399.7680

A Wave Digital Newton-Raphson Method for Virtual Analog Modeling of Audio Circuits with Multiple One-Port Nonlinearities

A. Bernardini, E. Bozzo, F. Fontana and A. Sarti, "A Wave Digital Newton-Raphson Method for Virtual Analog Modeling of Audio Circuits with Multiple One-Port Nonlinearities," in *IEEE/ACM Transactions on Audio, Speech, and Language Processing*,
doi: 10.1109/TASLP.2021.3084337.

Published in:
IEEE/ACM Transactions on Audio, Speech, and Language Processing

Document Version:
Postprint version

A Wave Digital Newton-Raphson Method for Virtual Analog Modeling of Audio Circuits with Multiple One-Port Nonlinearities

Alberto Bernardini, *Member, IEEE,* Enrico Bozzo,
Federico Fontana, *Senior Member, IEEE,* Augusto Sarti, *Senior Member, IEEE*

***Abstract*—The digital implementation of a nonlinear audio circuit often employs the Newton-Raphson (NR) method for solving the corresponding system of implicit ordinary differential equations in the discrete-time domain. Although its quadratic convergence speed makes NR attractive for real-time audio applications, quadratic convergence is not always guaranteed, since it depends on initial conditions, and also divergence might occur. For this reason, especially in the context of Virtual Analog modeling, techniques for increasing the robustness of NR are in order. Among the various approaches, the Wave Digital (WD) formalism recently showed potential to rethink traditional circuit simulation methods. In this manuscript, we discuss an original formulation of the NR method in the WD domain for the solution of audio circuits with multiple one-port nonlinearities. We provide an in-depth theoretical analysis of the proposed iterative method and we show how its quadratic convergence strongly depends on the free parameters (called port resistances) introduced when modeling the reference circuit in the WD domain. In particular, we demonstrate that the size of the basin where the WD NR solver can be initialized to converge on a solution with quadratic speed is a function of the free parameters. We also show that by setting each port resistance value as close as possible to the derivative w.r.t. current of the nonlinear element v–i characteristic we keep the basin size large. We finally implement an audio ring modulator circuit with four diodes in order to test the proposed iterative method.**

***Index Terms*—Wave Digital Filters, Nonlinear Audio Circuits, Newton-Raphson Method, Virtual Analog Modeling, Ring Modulator**

I. Introduction

THE digital modeling of analog audio circuits, often referred to as Virtual Analog modeling, has been an active and prolific research field in recent years [1]–[7]. In fact, audio and music technology are increasingly computerized and there is a strong need of emulating electronic musical instruments and analog audio effects by means of software capable of reproducing vintage sounds in a realistic and efficient fashion. The distinct sonic characteristics of most analog devices, such as guitar distortion effects or synthesizers, arise from their nonlinear behavior [3], [8] due to the presence of nonlinear circuit elements, such as diodes, transistors, and vacuum tubes. Virtual Analog modeling methods are often classified as *gray box* and *white box* [4]. Gray box modeling methods approximate the reference system with the input-output model that best fits circuit measurements; examples are Volterra-Wiener-Hammerstein models [9]–[11], neural networks [12], [13], and Legendre nonlinear filters [14]. White box modeling methods, instead, are based on the solution of the ordinary differential equations describing the actual audio circuit to be emulated; examples are state-space methods [15], [16], port-Hamiltonian methods [17], and Wave Digital Filters (WDFs) [2], [18]. Gray box modeling approaches are widely applicable and, usually, less computationally expensive than white box approaches, once the parameters of the model have been derived. White box models, however, are generally more accurate and their parameters do not need to be estimated, since they are usually available from the reference circuit schematic.

Among white box modeling approaches, WDFs [18] have been extensively used in the fields of both Virtual Analog modeling [2], [7], [19]–[24] and block-based sound synthesis through physical modeling [25], [26] in which audio systems are represented using electrical equivalents. The Wave Digital (WD) description of an electrical network is based on a port-wise consideration of the reference analog circuit and on a representation of circuit elements and topological junctions as input-output blocks characterized by scattering relations. In the Kirchhoff domain, every port of the circuit is identified by a pair of variables, namely a port voltage and a port current. Moving to the WD domain, each port voltage and port current pair is mapped into a pair of *wave variables* (an incident wave and a reflected wave) with the introduction at each port of a free parameter called reference port resistance or, simply, *port resistance* [18]. The free parameters are set so as to eliminate as many implicit relations (often called delay-free-loops in the literature [27]) as possible between port variables. As an example, in most WD realizations of one-port linear elements of interest, the local dependence between the wave incident to the element and the wave reflected from the element can be removed by properly setting the corresponding port resistance [18].

It follows that WDF principles allow us to compute dynamic circuits with up to one nonlinear element using a thoroughly explicit implementation, i.e., with no need to run iterative solvers, using stable discretization methods, such as Backward Euler and the trapezoidal rule [23], [24], [28]–[34]. This is not generally the case when we employ other circuit simulation strategies operating in the Kirchhoff domain, like modified

A. Bernardini and A. Sarti are with the Dipartimento di Elettronica, Informazione e Bioingegneria (DEIB), Politecnico di Milano; Piazza L. Da Vinci 32, 20133 Milano, Italy (e-mail: [alberto.bernardini,augusto.sarti]@polimi.it). E. Bozzo and F. Fontana are with the Department of Mathematics, Computer Science and Physics (DMIF), University of Udine; Via delle Scienze 206, 33100 Udine, Italy (e-mail: [enrico.bozzo,federico.fontana]@uniud.it).

nodal analysis methods [35], state-space methods [36] or port-Hamiltonian methods [17]. Such an advantage of WDF modeling, unfortunately, does not apply to reference circuits containing multiple nonlinearities because not all the delay-free-loops can be removed, and the use of iterative solvers is required also in the WD domain [37]. However, recent publications demonstrate that even in these cases working in the WD domain may be beneficial [23], [38]–[49].

Several fixed-point and Newton-Raphson (NR) methods have been developed so far for the solution of lumped circuits with multiple nonlinearities in the WD domain. It is known that an advantage of NR methods over fixed-point methods is that under certain circumstances NR methods converge with quadratic speed rather than the linear convergence speed characterizing fixed-point iterations. On the other hand, unlike fixed-point methods, NR methods require the computation of inverse Jacobian matrices. In [40], [41] a fixed-point method invoking the multi-dimensional WDF formalism [50] was developed. Another WD fixed-point method was proposed in [39] by Kabir *et al.* who noticed that "*the optimum selection of reference impedances* (port resistances) *at nonlinear device ports [. . .] may have to be adaptive since the optimum values are dependent on the circuit state.*". However, there were no systematic studies about the optimal selection of reference port resistances (free parameters) until the publication of the alternative WD fixed-point method, called Scattering Iterative Method (SIM), that was originally proposed in [44], [45] for the analysis of large nonlinear photovoltaic arrays and later extended in [23], [46], [47], [49] for the solution of dynamic nonlinear audio circuits. As far as the application of the NR method and variants thereof in the WD domain is concerned, Christoffersen proposed in [38] a hybrid scheme including fixed-point, NR method and Newton-Jacobi as particular cases, showing flexibility and efficiency in solving several nonlinear circuits in the WD domain. Other Newton's approximated schemes using the secant and pseudo-secant method applied to a diode clipper circuit with two diodes were then discussed in [42]. An NR method based on automatic differentiation is applied in [51] for solving the same circuit simulated in [42]. Further NR methods using backtracking and improved initial guesses proved to fit WD models of a diode clipper circuit and a circuit with a 2-port transistor in [43]. To the best of our knowledge, however, no publication presents a theoretical study on the optimization of port resistances in nonlinear WD networks in order to maximize the robustness and the convergence speed of the NR method.

This manuscript provides a first answer to the question about the best selection of port resistances while solving a circuit with multiple one-port nonlinearities in the WD domain using the NR method. We reconsider an approximation of a sufficient condition for quadratic convergence of the NR scheme that was recently derived in the Kirchhoff domain [52] from a known mathematical theorem [53]. Once expressed in the WD domain, such an approximation is used to infer values of port resistances that make the region of quadratic convergence large. Section II describes the WD networks that are the object of our investigation, and the way NR can be applied to their solution. Section III elaborates on the conditions of quadratic convergence of the proposed WD NR method. Section IV applies the theoretical tools provided in Section III to nonlinear networks with multiple diodes. As a case study, Section V discusses the robustness and the computational cost of the proposed WD NR method when employed for the solution of a ring modulator circuit. Section VI concludes this manuscript.

II. Modeling and Newton-Raphson Solution of WD Networks

A. WD Description of Circuits with One-Port Nonlinearities

We consider a reference electrical circuit composed of an arbitrary number N of linear or nonlinear one-port elements interconnected by a generic reciprocal lossless connection network. The class of reciprocal lossless connection networks includes purely topological interconnections made of wires, but also topological junctions that embed multi-port reciprocal lossless elements, such as ideal multi-winding transformers [54]. The reciprocal lossless connection network is implemented in the WD domain using an N-port scattering junction to which the N one-port WD elements are connected.

In the discrete-time domain, the scattering junction and the WD elements exchange voltage-wave signals expressed at every sampling step as follows

$$\mathbf{a} = \mathbf{v} + \mathbf{Z}\mathbf{i} \ , \quad \mathbf{b} = \mathbf{v} - \mathbf{Z}\mathbf{i} \ , \tag{1}$$

where the discrete-time index is omitted to avoid unnecessary complication of the notation, $\mathbf{v} = [v_1, \dots, v_N]^T$ is the vector of port voltages across the elements, $\mathbf{i} = [i_1, \dots, i_N]^T$ is the vector of port currents through the elements, $\mathbf{a} = [a_1, \dots, a_N]^T$ is the vector of waves reflected from the junction and incident to the elements, $\mathbf{b} = [b_1, \dots, b_N]^T$ is the vector of waves reflected from the elements and incident to the junction, and $\mathbf{Z} = \mathrm{diag}[Z_1, \dots, Z_N]$ is a diagonal matrix of positive-valued free parameters called *port resistances*. The superscript ^{T} denotes transposition.

At a given sampling step, in the domain of voltages and currents, referred to as *Kirchhoff domain*, the generic linear or nonlinear nth one-port element is characterized by a constitutive equation

$$\chi_n\left(v_n, i_n\right) = 0 \quad , \quad 1 \leq n \leq N \ , \tag{2}$$

where χ_n is a constant or time-varying linear or nonlinear scalar function. For a large class of linear elements, including resistive sources, resistors and linear capacitors or inductors that are discrete-time transformed using certain stable discretization methods (e.g., the trapezoidal method or the backward Euler method [23]), eq. (2) can be written in the form

$$v_n - R_{\mathrm{g}n} i_n - V_{\mathrm{g}n} = 0 \ , \tag{3}$$

where $V_{\mathrm{g}n}$ is a constant or time-varying voltage offset and $R_{\mathrm{g}n} > 0$ is a constant or time-varying resistance parameter.

According to (1), at each port n we have

$$v_n = \frac{a_n + b_n}{2} \ , \quad i_n = \frac{a_n - b_n}{2Z_n} \ . \tag{4}$$

Substituting (4) in (3) we get the linear scattering relation

$$b_n = \frac{R_{gn} - Z_n}{R_{gn} + Z_n} a_n + \frac{2Z_n}{R_{gn} + Z_n} V_{gn} \ . \tag{5}$$

We note that, by setting $Z_n = R_{gn}$, eq. (5) reduces to $b_n = V_{gn}$ and we remove the instantaneous dependency of b_n on a_n. This substitution is called *adaptation* in WDF theory [18].

In the more general case in which (2) is nonlinear, we assume that the substitution (4) in (2) leads to a corresponding scattering relation in the WD domain:

$$b_n = f_n\left(a_n\right) \ , \tag{6}$$

where f_n is a (nonlinear) scalar function that depends both on the incident wave a_n and the free parameter Z_n. In order to simplify notation, the dependence on Z_n is not made explicit. Moreover, without loss of generality we have assumed (6) to be in explicit form.

We then express the N scattering relations (one for each one-port circuit element) in vector form as

$$\mathbf{b} = \begin{bmatrix} b_1 \\ \vdots \\ b_N \end{bmatrix} = \begin{bmatrix} f_1(a_1) \\ \vdots \\ f_N(a_N) \end{bmatrix} = \mathbf{f}(\mathbf{a}) \ . \tag{7}$$

On the other hand, the reciprocal lossless connection network, containing all the topological information of the circuit, is implemented in the WD domain using a junction characterized by a $N \times N$ scattering matrix $\mathbf{S}$ such that

$$\mathbf{a} = \mathbf{S}\mathbf{b} \ . \tag{8}$$

As discussed in the literature [54], the scattering matrix of a reciprocal lossless WD junction based on the definition (1) is characterized by two special properties: the *self-inverse property* and the *losslessness property*. According to the self-inverse property, $\mathbf{S}$ is involutory, i.e.,

$$\mathbf{S}\mathbf{S} = \mathbf{I} \tag{9}$$

where $\mathbf{I}$ is the identity matrix. According to the losslessness property, instead, $\mathbf{S}$ satisfies

$$\mathbf{S}^T \mathbf{Z}^{-1} \mathbf{S} = \mathbf{Z}^{-1} \ , \tag{10}$$

where the diagonal matrix $\mathbf{Z}^{-1}$ is the inverse of $\mathbf{Z}$.

Combining (7) and (8) we obtain the following vectorial equation that describes the WD network in terms of the incident waves,

$$\mathbf{a} - \mathbf{S}\mathbf{f}(\mathbf{a}) = \mathbf{0} \ , \tag{11}$$

where $\mathbf{0}$ is a $N \times 1$ column vector of zeros. It is worth noticing that, since $\mathbf{S}$ is involutory by (9) we can equivalently rewrite (11) as

$$\mathbf{S}\mathbf{a} - \mathbf{f}(\mathbf{a}) = \mathbf{0} \ . \tag{12}$$

If more than one circuit element is nonlinear then the system (12) is characterized by implicit equations, and the unknown vector variable $\mathbf{a}$ needs to be estimated at each sampling step employing approximation methods that are usually iterative. In the next section we discuss the case when an NR solver is used.

B. Proposed WD Newton-Raphson Solver

Let us define the nonlinear vector function $\mathbf{g}(\mathbf{a}) = [g_1(\mathbf{a}), \ldots, g_N(\mathbf{a})]^T$, according to (12), as

$$\mathbf{g}(\mathbf{a}) = \mathbf{S}\mathbf{a} - \mathbf{f}(\mathbf{a}) \ , \tag{13}$$

and its Jacobian matrix as

$$\mathbf{J}_{\mathbf{g}}\left(\mathbf{a}\right) = \mathbf{S} - \mathbf{J}_{\mathbf{f}}(\mathbf{a}) \ , \tag{14}$$

where $\mathbf{J}_{\mathbf{f}}(\mathbf{a})$ is the Jacobian of the vector function $\mathbf{f}(\mathbf{a})$. Both $\mathbf{J}_{\mathbf{g}}(\mathbf{a})$ and $\mathbf{J}_{\mathbf{f}}(\mathbf{a})$ are $N \times N$ matrices whose entries depend on the incident waves in vector $\mathbf{a}$. In particular, we have that

$$\mathbf{J}_{\mathbf{f}}\left(\mathbf{a}\right) = \mathrm{diag}\left[f_1'(a_1), \ldots, f_N'(a_N)\right] \tag{15}$$

where

$$f_n'(a_n) = \frac{\mathrm{d}f_n(a_n)}{\mathrm{d}a_n} \tag{16}$$

is the derivative of f_n with respect to a_n.

An NR solution of (12) can be obtained by iteratively computing the following update rule, starting with an initial guess $\mathbf{a}^{(0)}$,

$$\mathbf{a}^{(\gamma)} = \mathbf{a}^{(\gamma-1)} - \mathbf{J}_{\mathbf{g}}^{-1}\big(\mathbf{a}^{(\gamma-1)}\big)\left(\mathbf{S}\,\mathbf{a}^{(\gamma-1)} - \mathbf{f}\big(\mathbf{a}^{(\gamma-1)}\big)\right) \ , \tag{17}$$

where $\mathbf{a}^{(\gamma)}$ is the outcome of the γth iteration. The stop condition is

$$\|\mathbf{v}^{(\gamma)} - \mathbf{v}^{(\gamma-1)}\| < \xi_{\text{WDNR}} \ , \tag{18}$$

where $\|\cdot\|$ is the Euclidean norm, ξ_{WDNR} is a small tolerance (that in this manuscript is set as $\xi_{\text{WDNR}} = 10^{-8}$), while $\mathbf{v}^{(\gamma)}$ is the vector of port voltages computed at the γth NR iteration and defined by (4) as

$$\mathbf{v}^{(\gamma)} = \frac{1}{2}\left(\mathbf{a}^{(\gamma)} + \mathbf{f}\big(\mathbf{a}^{(\gamma)}\big)\right) \ . \tag{19}$$

Generally, the closer the initial guess to the solution, the faster the NR convergence. In our case, the initial guess $\mathbf{a}^{(0)}[k]$ at sampling step $k > 1$ can be set by substituting the most recent values of $\mathbf{v}$, $\mathbf{i}$ and $\mathbf{Z}$ in (1):

$$\mathbf{a}^{(0)}[k] = \mathbf{v}[k-1] + \mathbf{Z}[k]\mathbf{i}[k-1] \tag{20}$$

where $\mathbf{v}[k-1]$ and $\mathbf{i}[k-1]$ are the vector of port voltages and the vector of port currents found at the previous sampling step $k-1$, while $\mathbf{Z}[k]$ is the diagonal matrix of free parameters at sampling step k. As far as the sampling step $k = 1$ is concerned, the initial guess should be set according to the initial conditions of the circuit. A discussion on how to set initial conditions in WD structures can be found in [29]. However, in most scenarios of interest in Virtual Analog modeling, we assume that the circuit is off at the sampling step $k = 0$; therefore Kirchhoff port variables are initialized to zero, i.e., $\mathbf{v}[0] = \mathbf{i}[0] = \mathbf{0}$. Since, according to (20), we would have that $\mathbf{a}^{(0)}[1] = \mathbf{0}$, and a zero-valued seed vector might cause numerical problems to NR, we set $\mathbf{a}^{(0)}[1] = [\epsilon_1, \ldots, \epsilon_N]^T$, where $\epsilon_1, \ldots, \epsilon_N$ are small voltage values, e.g., $\epsilon_1 = \cdots = \epsilon_N = 0.1$ V.

III. Quadratic Convergence Conditions of the WD Newton-Raphson Solver

In the following derivation, for simplicity, we will refer to the current-to-voltage characteristic of a one-port element of the reference circuit generally as $v(i)$. Thus, the incident and the reflected waves (1) of a generic one-port element can be observed as functions of the current i, respectively h_a and h_b:

$$a = v(i) + Zi = h_a(i) \ , \ b = v(i) - Zi = h_b(i). \tag{21}$$

Let us assume that each one-port element is characterized by a monotonically increasing current-to-voltage characteristic, i.e.,

$$v'(i) > 0 \ . \tag{22}$$

This assumption is satisfied by all linear elements whose discrete-time model can be put in the form (3) if $R_{gn} > 0$ at every sampling step. Assumption (22) is also satisfied by nonlinear diodes characterized by the Shockley exponential model and one-port nonlinearities with memoryless saturation characteristics, e.g., pairs of exponential diodes in anti-parallel.

Eq. (21), combined with (22) and with the further assumption that

$$Z > 0 \ , \tag{23}$$

implies that the function $h_a(i)$ is monotonic, hence invertible. From here, $b = f(a) = h_b\big(h_a^{-1}(a)\big)$. Deriving the composition $h_a^{-1} \circ h_b$ yields

$$f'(a) = \frac{h_b'\big(h_a^{-1}(a)\big)}{h_a'\big(h_a^{-1}(a)\big)} = \frac{v'(i) - Z}{v'(i) + Z}. \tag{24}$$

Conditions (22) and (23) applied to (24) imply also

$$|f'(a)| < 1 \ . \tag{25}$$

Deriving (24) we get

$$\begin{aligned} f''(a) &= \frac{\frac{h_b''(h_a^{-1}(a))}{h_a'(h_a^{-1}(a))} h_a'\big(h_a^{-1}(a)\big) - \frac{h_b'(h_a^{-1}(a)) h_a''(h_a^{-1}(a))}{h_a'(h_a^{-1}(a))}}{h_a'\big(h_a^{-1}(a)\big)^2} \\ &= \frac{h_b''\big(h_a^{-1}(a)\big) h_a'\big(h_a^{-1}(a)\big) - h_b'\big(h_a^{-1}(a)\big) h_a''\big(h_a^{-1}(a)\big)}{h_a'\big(h_a^{-1}(a)\big)^3} \\ &= \frac{v''(i)\big(v'(i) + Z\big) - \big(v'(i) - Z\big) v''(i)}{\big(v'(i) + Z\big)^3} \\ &= \frac{2Z v''(i)}{\big(v'(i) + Z\big)^3}. \end{aligned} \tag{26}$$

In [52], a sufficient condition for quadratic convergence of NR has been discussed, along with an approximated and more tractable version of it. Such a simplified condition makes use of $\mathbf{H_g}(\mathbf{a})$, a matrix in which every element (n, j) is the second derivative of g_n with respect to a_j, $1 \le n, j \le N$. In our case, given (13), (14), and (15), matrix $\mathbf{H_g}(\mathbf{a})$ can be written as

$$\mathbf{H_g}\left(\mathbf{a}\right) = -\mathrm{diag}\big[f_1''(a_1), \ldots, f_N''(a_N)\big]. \tag{27}$$

Let us consider a hypersphere centered on a solution point $\mathbf{a}$ and with radius $1/M(\mathbf{a})$ such that

$$M(\mathbf{a}) = \frac{1}{2}\big\|\mathbf{J_g}^{-1}(\mathbf{a})\mathbf{H_g}(\mathbf{a})\big\|_\infty \le \frac{\sqrt{N}}{2}\big\|\mathbf{J_g}^{-1}(\mathbf{a})\mathbf{H_g}(\mathbf{a})\big\| \tag{28}$$

where the operators $\|\cdot\|_\infty$ and $\|\cdot\|$ indicate the infinity matrix norm and the Euclidean matrix norm, respectively. The inequality in (28) holds because of the equivalence between the infinity matrix norm and the Euclidean matrix norm [55]. The simplified condition discussed in [52] states that there exists a *basin* around $\mathbf{a}$ and included inside the aforementioned hypersphere where the NR solver can be initialized to converge on the solution $\mathbf{a}$ with quadratic speed. According to the experimental results in [52], the larger $1/M(\mathbf{a})$, the larger the basin of quadratic convergence. We will therefore elaborate on expression (28) to infer port resistance values (free parameters Z_n) that keep the size of this basin large, as a possibility to speed up the convergence.

First of all, if condition (25) descending from (24) holds for each one-port element then $\mathbf{J_g}(\mathbf{a})$ has an inverse. This is proved in Appendix A. This inverse is such that

$$\big\|\mathbf{J_g}^{-1}(\mathbf{a})\big\| \le \sqrt{\frac{Z_{\max}}{Z_{\min}}} \frac{1}{1 - \big\|\mathbf{J_f}(\mathbf{a})\big\|}, \tag{29}$$

in which $\big\|\mathbf{J_f}(\mathbf{a})\big\| < 1$, and $Z_{\max}$ and $Z_{\min}$ are respectively the largest and smallest port resistance. Hence,

$$M(\mathbf{a}) \le \frac{\sqrt{N}}{2}\sqrt{\frac{Z_{\max}}{Z_{\min}}} \frac{\big\|\mathbf{H_g}(\mathbf{a})\big\|}{1 - \big\|\mathbf{J_f}(\mathbf{a})\big\|}. \tag{30}$$

Eqs. (29) and (30) are proved in Appendix B.

We can minimize the upper bound in (30) by simultaneously minimizing its numerator and maximizing its denominator. The latter operation is straightforward. In fact, by (15) and (24), $\big\|\mathbf{J_f}(\mathbf{a})\big\|$ can be set to zero by choosing

$$Z_n = v_n'(i_n) \tag{31}$$

for each $1 \le n \le N$, that is, at each port of the WD network.

The same upper limit depends also on the second-order derivatives $f_n''(a_n)$, through $\big\|\mathbf{H_g}(\mathbf{a})\big\|$. When (31) is used to maximize the denominator of the upper bound, then (30) becomes, by substituting $Z_n = v_n'(i_n)$ in (27) through (26),

$$\begin{aligned} M(\mathbf{a}) &\le \frac{\sqrt{N}}{2}\sqrt{\frac{Z_{\max}}{Z_{\min}}}\big\|\mathbf{H_g}(\mathbf{a})\big\| \\ &= \frac{\sqrt{N}}{8}\sqrt{\frac{\max\limits_{1\le n\le N} v_n'(i_n)}{\min\limits_{1\le n\le N} v_n'(i_n)}} \max_{1\le n\le N} \frac{\big|v_n''(i_n)\big|}{[v_n'(i_n)]^2}. \end{aligned} \tag{32}$$

In principle there is no guarantee that condition (31) minimizes (30). For this reason, this choice remains heuristic. On the other hand (31) is especially attractive besides its simplicity, as it generalizes the principle of linear one-port element adaptation known in traditional WDF theory [18] to nonlinear one-port elements as soon as their instantaneous current-to-voltage characteristics are monotonically increasing. In fact, even for linear one-ports characterized by a constitutive equation in the form (3) the adaptation condition is $Z_n = R_{gn} = v_n'(i_n)$. As a further consideration, please note that for linear one-ports condition $f_n''(a_n) = 0$ always holds, implying by (27) that the radius $1/M(\mathbf{a})$ is infinitely large in a fully linear WD network. As a matter of fact, if all one-ports are linear and condition (31) is applied then NR converges in just one iteration. In light of these considerations (30) suggests

that, by choosing the same condition (31) if one or more nonlinearities are present, NR converges with high speed to the equilibrium point of the network at every sampling step.

Even more interestingly, a similar result in terms of optimal values of port resistances has been found when a fixed-point method, instead of NR, was used in [23], [44]–[46], [49] for solving circuits with multiple nonlinear one-port elements. In fact, in references [44] and [49], the convergence analyses of the WD fixed-point iterative solver, called SIM, show that the free parameter (port resistance) of each one-port should be set as close as possible to the slope of the tangent line intersecting the operating point on its v–i characteristic, i.e., $Z_n = v_n'(i_n)$, in order to increase speed of convergence as much as possible.

Moreover, it is worth noting that, in this manuscript, there is no quantitative expression putting the size of the basin in relation with the speed of convergence. Though, there is ample evidence that the larger the basin, the faster the convergence is [52]. For instance, as we have already seen, in a linear WD network the radius $1/M(\mathbf{a})$ is infinitely large and NR would hit the solution always in one step. Holding this evidence, the factors $\sqrt{N}$ and $\sqrt{Z_{\max}/Z_{\min}}$ in the upper bound of $M(\mathbf{a})$ are also expected to condition the NR convergence speed.

Finally, it must be always considered that condition (31) can never be set exactly, as all the port currents and the port voltages of the network become apparent *after* the computation through NR of the vector $\mathbf{a}$ of incident waves. Keeping robustness and efficiency in mind, a reasonable estimation of the values $v_n'(i_n)$ can be made using the port variables at the previous sampling steps when setting the current port resistances.

IV. Application of Convergence Analysis to Circuits with Multiple Diodes

In this section we discuss how the general convergence analysis described in the previous section can be applied to circuits containing multiple nonlinear diodes. We consider two different models: the *Shockley diode* and the *extended Shockley diode*, i.e., the Shockley model augmented with a series resistor and a parallel resistor. In both cases we make sure that the v–i characteristic is monotonically increasing, then we provide mathematical expressions that are useful to delimit the basin of quadratic convergence. Finally, for both models we derive explicit WD scattering equations.

A. Shockley diode model case

The well-known Shockley diode model is characterized by the constitutive equation

$$i - I_{\mathrm{s}}(e^{v/\beta} - 1) = 0 \tag{33}$$

where e is the Napier's constant, i is the port current, v is the port voltage, I_{s} is the saturation current, and the parameter $\beta = \eta V_{\mathrm{t}}$ denotes the thermal voltage V_{t} multiplied by the p-n junction ideality factor η. The port voltage can be expressed by turning (33) into a function of the port current:

$$v(i) = \beta \ln\left(1 + \frac{i}{I_{\mathrm{s}}}\right) \ . \tag{34}$$

From here,

$$v'(i) = \frac{\beta}{I_{\mathrm{s}} + i} \ . \tag{35}$$

Since $\beta > 0$, $I_{\mathrm{s}} > 0$ and $i > -I_{\mathrm{s}}$, then (22) holds; it follows that (34) is monotonically increasing. Deriving (35) again, we get

$$v''(i) = -\frac{\beta}{(I_{\mathrm{s}} + i)^2} \ . \tag{36}$$

Hence, by (31), the port resistance of a WD Shockley diode model is set as

$$Z = v'(i) = \frac{\beta}{I_{\mathrm{s}} + i} \ . \tag{37}$$

Holding this choice, using (35) and (36), the ratio

$$\frac{\left|v''(i)\right|}{[v'(i)]^2} = \frac{1}{\beta} \tag{38}$$

is useful for evaluating the upper limit in (32). Under the assumption that all the nonlinear one-ports of the circuit are identical diodes characterized by the same Shockley model, and remembering that for linear one-port elements we have $v_n''(i_n) = 0$, (32) reduces to

$$M(\mathbf{a}) \leq \frac{\sqrt{N}}{8\beta} \sqrt{\frac{Z_{\max}}{Z_{\min}}} \ . \tag{39}$$

Although not necessary for the convergence analysis of the WD NR solver, here we also provide an explicit WD scattering equation which can be used for computing the WD Shockley diode model. This equation, based on the Lambert W function, was already presented in [19], [32], [56] and is rewritten here in terms of the Wright ω function [57], which is defined as $\omega(z) = \mathrm{W}(e^z)$ with $z \in \mathbb{R}$. The WD Shockley diode scattering function is

$$f(a) = a + 2ZI_{\mathrm{s}} - 2\beta\,\omega\big(\varphi(a)\big) \ , \tag{40}$$

where

$$\varphi(a) = \frac{ZI_{\mathrm{s}} + a}{\beta} + \log\Big(\frac{ZI_{\mathrm{s}}}{\beta}\Big) \ .$$

The first- and second-order derivatives of (40) can also be expressed in closed-form as follows:

$$f'(a) = 1 - \frac{2\,\omega\big(\varphi(a)\big)}{1 + \omega\big(\varphi(a)\big)} \ , \tag{41}$$

$$f''(a) = \frac{-2\,\omega\big(\varphi(a)\big)}{\beta\Big(1 + \omega\big(\varphi(a)\big)\Big)^3} \ . \tag{42}$$

B. Extended Shockley diode model case

The Shockley model of a p-n junction diode is usually accurate only for relatively small voltage values. Large negative values cause current leaks in parallel to saturation; conversely, large positive voltages cause the diode to resist from excessive current flow across itself. Such effects are modeled by adding one resistor with large resistance $R_{\mathrm{P}} > 0$ in parallel and one resistor with small resistance $R_{\mathrm{S}} > 0$ in series to the Shockley diode [23], [46]. The resulting v–i characteristic hence obeys to the following implicit relation

$$i - I_{\mathrm{s}}\left(e^{\frac{v(i) - R_{\mathrm{S}} i}{\beta}} - 1\right) - \frac{v(i) - R_{\mathrm{S}}\, i}{R_{\mathrm{P}}} = 0 \ , \tag{43}$$

where $v(i)$ and i are the port voltage and the port current of the one-port model that will be referred to as *extended Shockley diode model*. The use of additional resistors also prevents numerical problems that often arise when using the Shockley diode model whose v–i curve is characterized by extremely high (and extremely low) slopes, especially when dealing with large-amplitude signals [23], [46]. It is therefore useful to check whether the v–i characteristic of the extended Shockley diode model has a positive derivative. If this is true, then we can apply the convergence analysis of Section III also in this case.

Let us define the function $y(i) = \big(v(i) - R_\mathrm{S} i\big)/\beta$, later simply referred to as y. From here, (43) can be rewritten as

$$I_\mathrm{s} e^{y} - I_\mathrm{s} + \frac{\beta}{R_\mathrm{P}} y = i. \tag{44}$$

This relationship confirms that $y(0) = v(0) = 0$, and also implies that $\lim_{i\to\pm\infty} y = \pm\infty$. Now, by deriving (44) with respect to i we get

$$I_\mathrm{s} y' e^{y} + \frac{\beta}{R_\mathrm{P}} y' = y'\big(I_\mathrm{s} e^{y} + \frac{\beta}{R_\mathrm{P}}\big) = 1, \tag{45}$$

where y' denotes the derivative of y with respect to i and can be written as

$$y' = \frac{1}{I_\mathrm{s} e^{y} + \frac{\beta}{R_\mathrm{P}}}. \tag{46}$$

Eq. (46) shows that $0 < y' = \frac{v'(i) - R_\mathrm{S}}{\beta} < \frac{R_\mathrm{P}}{\beta}$, so that $R_\mathrm{S} < v'(i) < R_\mathrm{S} + R_\mathrm{P}$. Hence, $v'(i) > 0$ for every current; this means that $v(i)$ is monotonically increasing. $y'(i)$ is always positive, too, furthermore it decreases from R_P/β until zero in the range $(-\infty, +\infty)$ of i. Then, more precisely, $v'(i) = \beta y'(i) + R_\mathrm{S}$ decreases from $R_\mathrm{P} + R_\mathrm{S}$ to R_S in the same range. This characteristic behavior is self-evident by inspecting (43) in particular when $i = \pm\infty$.

By computing the derivative with respect to i of both members of equation (45) we get

$$y''\big(I_\mathrm{s} e^{y} + \frac{\beta}{R_\mathrm{P}}\big) + I_\mathrm{s} (y')^2 e^{y} = 0, \tag{47}$$

that, by moving the second term to the right and then using (46) and (45), becomes

$$\frac{y''}{y'} = y'\big(\frac{\beta}{R_\mathrm{P}} y' - 1\big). \tag{48}$$

Hence, we get

$$y'' = \frac{v''}{\beta} = (y')^2 \big(\frac{\beta}{R_\mathrm{P}} y' - 1\big). \tag{49}$$

Along with recalling that $0 < y' < R_\mathrm{P}/\beta$, eq. (49) proves that y'' and v'' are always negative. This conclusion, again by (49), implies that $v'(i)$ is not only positive and decreasing as we have already seen, but also monotonically decreasing.

By rewriting y and y' respectively as functions of $v(i)$, according to (46), $v'(i)$ can be written as

$$v'(i) = \frac{\beta(R_\mathrm{S} + R_\mathrm{P}) + R_\mathrm{S} R_\mathrm{P} I_\mathrm{s} e^{\frac{v(i) - R_\mathrm{S} i}{\beta}}}{\beta + R_\mathrm{P} I_\mathrm{s} e^{\frac{v(i) - R_\mathrm{S} i}{\beta}}}\ . \tag{50}$$

Expression (50), that can also be obtained by directly applying the implicit function theorem to (44), is explicitly computable only if both i and $v(i)$ are known.

Given (49), we can also express $v''(i)$ as

$$v''(i) = -\frac{\beta R_\mathrm{P}^3 I_\mathrm{s}\, e^{\frac{v(i) - R_\mathrm{S} i}{\beta}}}{\Big(\beta + R_\mathrm{P} I_\mathrm{s} e^{\frac{v(i) - R_\mathrm{S} i}{\beta}}\Big)^3}\ . \tag{51}$$

We derived all the analytical expressions needed for computing the upper bound of the basin $M(\mathbf{a})$ in equation (30) dealing with circuits with multiple nonlinearities characterized by the extended Shockley diode model. Again, the upper bound is kept low according to (31) by setting $Z = v'(i)$ for each element. Using (50) and (51), the ratio

$$\frac{\big|v''(i)\big|}{[v'(i)]^2} = \frac{\beta R_\mathrm{P}^3 I_\mathrm{s}\, e^{y(i)}}{\big(\beta + R_\mathrm{P} I_\mathrm{s} e^{y(i)}\big)\big(\beta(R_\mathrm{S} + R_\mathrm{P}) + R_\mathrm{S} R_\mathrm{P} I_\mathrm{s} e^{y(i)}\big)^2} \tag{52}$$

turns useful for evaluating the upper limit in (32). It can be verified that when I_s and R_S are small and R_P is large, for sufficiently low values of port current i, (52) is well approximated by (38).

Like in the case of the Shockley diode, we also provide an explicit WD scattering function that characterizes the extended Shockley diode model:

$$f(a) = \frac{2Z R_\mathrm{P} I_\mathrm{s} + a(R_\mathrm{P} + R_\mathrm{S} - Z)}{Z + R_\mathrm{P} + R_\mathrm{S}} - \frac{2\beta Z}{Z + R_\mathrm{S}} \omega\big(\varphi(a)\big) \tag{53}$$

where

$$\varphi(a) = \frac{a R_\mathrm{P} + R_\mathrm{P} I_\mathrm{s}\,(Z + R_\mathrm{S})}{\beta\,(Z + R_\mathrm{P} + R_\mathrm{S})} + \log\left(\frac{R_\mathrm{P} I_\mathrm{s}\,(Z + R_\mathrm{S})}{\beta\,(Z + R_\mathrm{P} + R_\mathrm{S})}\right)\ .$$

Closed-form expressions of the first- and second-order derivatives of (53) are:

$$f'(a) = \frac{R_\mathrm{P} + R_\mathrm{S} - Z}{R_\mathrm{P} + R_\mathrm{S} + Z} - \\ + \frac{2R_\mathrm{P} Z\, \omega\big(\varphi(a)\big)}{(R_\mathrm{S} + Z)(R_\mathrm{P} + R_\mathrm{S} + Z)\Big(1 + \omega\big(\varphi(a)\big)\Big)}\ , \tag{54}$$

$$f''(a) = \frac{-2Z R_\mathrm{P}^2\, \omega\big(\varphi(a)\big)}{\beta(R_\mathrm{S} + Z)(R_\mathrm{P} + R_\mathrm{S} + Z)^2\Big(1 + \omega\big(\varphi(a)\big)\Big)^3}\ . \tag{55}$$

V. Case Study: Ring Modulator

In this section we apply the proposed WD NR method to a signal modulator containing a ring circuit made of four diodes. Invented by Cowan [58] in the thirties and originally used as a heterodyning element in single-sideband communications systems [59], the ring modulator has been widely adopted as an audio effect by electronic music composers such as K. Stockhausen, by the BBC Radiophonic workshop, and by sound synthesizer manufacturers including Buchla, Moog, Oberheim, and Bode [60], [61]. In the literature on Virtual Analog modeling, several works present simplified or accurate models of diode-based ring modulator circuits [23], [32], [46], [52], [60], [62], [63]. Here we consider the ring modulator

TABLE I
RING MODULATOR: PORT RESISTANCES OF LINEAR ELEMENTS

Port Res.	Value	Port Res.	Value	Port Res.	Value
Z_5	$\frac{2L_\mathrm{A}}{T_\mathrm{s}}$	Z_8	$\frac{T_\mathrm{s}}{2C_\mathrm{B}}$	Z_{11}	R_d
Z_6	$\frac{2L_\mathrm{B}}{T_\mathrm{s}}$	Z_9	$\frac{T_\mathrm{s}}{2C_\mathrm{d}}$	Z_{12}	R_out
Z_7	$\frac{T_\mathrm{s}}{2C_\mathrm{A}}$	Z_{10}	R_in	Z_{13}	R_c

circuit in Fig. 1, already discussed in [23], [52], [62]. This circuit is characterized by two ideal 3-winding transformers, whose turn ratios are $\theta/\mu = \gamma/\mu = \xi/\lambda = \tau/\lambda = 1/2$, where θ, γ, μ, ξ, τ and λ are the numbers of turns in each winding. The input signal and the carrier signal are both sinusoids in the forms $V_\mathrm{in}(t) = A_\mathrm{in}\sin(2\pi f_\mathrm{in} t)$ and $V_\mathrm{c}(t) = A_\mathrm{c}\sin(2\pi f_\mathrm{c} t)$, where t is the continuous-time variable in seconds, f_in and f_c are the fundamental frequencies in Hz of the input and the carrier, respectively, while A_in and A_c are voltage amplitudes. The output signal V_out is the voltage across the resistor R_out. The parameters of the linear one-port elements and the corresponding values are: $L_\mathrm{A} = L_\mathrm{B} = 0.8$ H, $C_\mathrm{A} = C_\mathrm{B} = C_\mathrm{d} = 1$ nF, $R_\mathrm{d} = 50\ \Omega$, $R_\mathrm{in} = 80\ \Omega$, $R_\mathrm{c} = 1\ \Omega$ and $R_\mathrm{out} = 600\ \Omega$. All four nonlinear diodes are identical, and they are modeled with the extended Shockley diode model discussed in Subsection IV-B; their parameters and corresponding values are: $I_\mathrm{s} = 1$ nA, $\eta = 2.19$, $V_\mathrm{t} = 26$ mV, $R_\mathrm{S} = 1$ mΩ and $R_\mathrm{P} = 100$ kΩ.

The WD realization of the circuit in Fig. 1 is shown in Fig. 2. The WD structure is characterized by 13 one-port elements and a single 13-port junction embedding the two 3-winding transformers. The WD junction realizes a reciprocal lossless connection network [23], [54], [64], hence its scattering matrix $\mathbf{S}$ can be computed as

$$\mathbf{S} = 2\mathbf{Q}^T \left(\mathbf{Q}\mathbf{Z}^{-1}\mathbf{Q}^T\right)^{-1} \mathbf{Q}\mathbf{Z}^{-1} - \mathbf{I}_{13} \tag{56}$$

where $\mathbf{Z} = \mathrm{diag}[Z_1, \ldots, Z_{13}]$ is the diagonal matrix of port resistances, $\mathbf{I}_{13}$ is the 13×13 identity matrix while $\mathbf{Q} = [\mathbf{F}, \mathbf{I}_4]$, being $\mathbf{I}_4$ the 4×4 identity matrix and

$$\mathbf{F} = \begin{bmatrix} 0.5 & 0.5 & -0.5 & -0.5 & 1 & 0 & 1 & 0 & 0 \\ 1 & -1 & 1 & -1 & 0 & 0 & 0 & 0 & 0 \\ -0.5 & 0.5 & 0.5 & -0.5 & 0 & 1 & 0 & 1 & 0 \\ 1 & -1 & 1 & -1 & 0 & 0 & 0 & 0 & 1 \end{bmatrix}.$$

The linear elements can be modeled using eq. (5). Each linear element is adapted [18], i.e., the local instantaneous dependency of the reflected wave variable on the incident wave variable has been removed. The continuous-time derivatives in the constitutive equations of capacitors and inductors are approximated using the trapezoidal rule as in traditional WDFs [18]. The chosen sampling frequency is $F_\mathrm{s} = 1/T_\mathrm{s} = 44.1$ kHz. The WD realization of nonlinear diodes is based on the scattering relation in eq. (53). The Wright function $\omega(x)$ in eq. (53) is implemented using the method presented in [65]. The port resistances of the adapted linear elements are reported in Table I. The choice of the port resistances $Z_1, \ldots, Z_4$ of the nonlinear diodes is the main point of interest in this case study. According to the considerations presented in Section III and Section IV a good choice for the port resistances of both linear and nonlinear elements characterized by a monotonically increasing v–i characteristic is $Z_n = v_n'(i_n)$. It can be easily verified, using eq. (3), that the port resistances of linear elements (adapted according to traditional WDF principles) already satisfy condition (31), i.e., $Z_n = v_n'(i_n) = R_{\mathrm{g}n}$. As far as nonlinear elements are concerned, their derivative $v_n'(i_n)$ can be estimated at each sampling step before solving the circuit by using the respective value at the previous sample.

A. First Experiment

In a first experiment we simulate the ring modulator circuit using the proposed WD NR method based on the update rule (17). At every sampling step, each of the free parameters $Z_1, \ldots, Z_4$ is set equal to the slope of the tangent line intersecting the operating point on the v–i characteristic of the corresponding element at the previous step. The output signals resulting from two different simulations are reported in Fig. 3. The upper plot of Fig. 3 refers to a simulation in which we set the parameters of the input signal as $g_\mathrm{in} = 5$ V and $f_\mathrm{in} = 1500$ Hz, while the parameters of the carrier signal as $g_\mathrm{c} = 5$ V and $f_\mathrm{c} = 500$ Hz. The lower plot refers to another simulation in which we set $g_\mathrm{in} = 5$ V, $f_\mathrm{in} = 1500$ Hz, $g_\mathrm{c} = 5$ V and $f_\mathrm{c} = 810$ Hz. A comparison to the results obtained with LTspice simulations confirms the accuracy of the WD implementations. Despite the high level of distortion of the output signal due to the high amplitude and the high fundamental frequency of the input signals, the proposed WD NR method always converges to the correct solution. Other simulations with parameters f_c and f_in varied up to 15 kHz and parameters g_c and g_in varied up to 10 V have been performed; the proposed WD NR method always converged to the correct solution.

B. Second Experiment

In a second experiment the values of $v_n'(i_n)$ at every sampling step are precomputed in ways that they can be assigned to the free parameters Z_n at ports $1, \ldots, 4$ during the simulation. In this way the performance of the WD NR method is tested in the ideal case, as if $v_n'(i_n)$ was known a priori. After setting the parameters of the input signals as in the first simulation of the previous experiment, i.e., $g_\mathrm{in} = 5$ V, $f_\mathrm{in} = 1500$ Hz, $g_\mathrm{c} = 5$ V and $f_\mathrm{c} = 500$ Hz, we performed many simulations while progressively shifting the values of the port resistances Z_n away from their reference value $v_n'(i_n)$. The results are shown in Fig. 4. In both subfigures of Fig. 4, blue circles represent the average number of NR iterations (upper plot) and the maximum number of NR iterations (lower plot) for different settings of the free parameters $Z_1, \ldots, Z_4$. On the x-axis of each plot we have the deviation in percentage with respect to the reference setting in which $Z_n = v_n'(i_n)$. Different ranges of deviation are considered in the two subfigures.

Fig. 4(a) shows the result of 200 simulations in the deviation range $[-99.9\%, 99.9\%]$. Reducing the free parameters Z_n by 100% (-100% case) would have been equivalent to setting $Z_1 = Z_2 = Z_3 = Z_4 = 0$; therefore, since in this manuscript

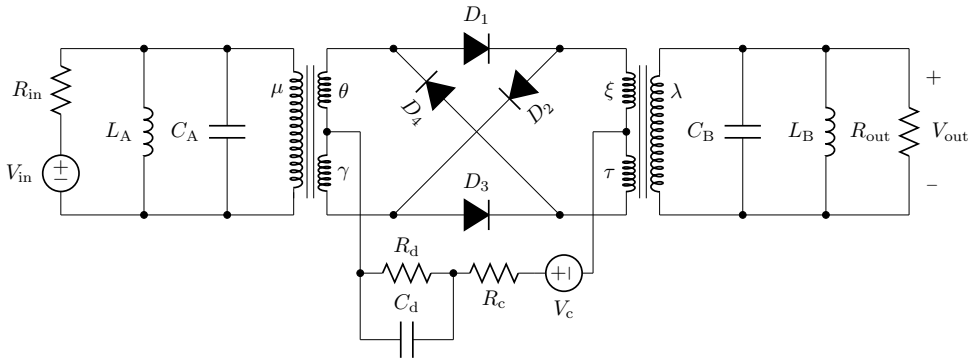

Fig. 1. Dynamic ring modulator circuit.

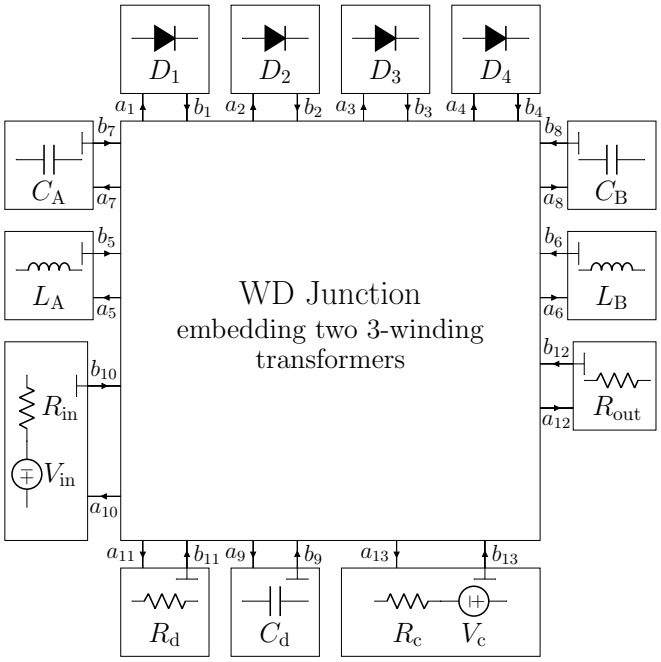

Fig. 2. WD structure corresponding to the circuit in Fig. 1.

we assume that $Z_n > 0$, we take -99.9% as the lowest limit of the deviation range. In both the upper and the lower plot, the absolute minimum occurs when $Z_n = v_n'(i_n)$; in the 0% of deviation case, in fact, we get the smallest average number of NR iterations, which is 4.41, and the smallest maximum number of NR iterations, which is 7. We can clearly see how the average number and the maximum number of NR iterations progressively increase when the values of the free parameters are decreased; when the values of the free parameters are increased, instead, they stay almost flat.

Fig. 4(b) shows the result of 100 simulations in the deviation range $[10^{-4}\%, 10^{8}\%]$ represented in logarithmic scale. We notice that a local minimum is reached when $Z_n \simeq 10 \times v_n'(i_n)$ (corresponding to an increase of almost 1000% w.r.t. the reference); in that case, the average number of NR iterations is 4.67 and the maximum number of NR iterations is 8. It is evident that, after the aforementioned local minimum, the average and the maximum number of NR iterations keep increasing while the values of the free parameters are increased. The red asterisks on the x-axis in Fig. 4(b) refer to simulations in which the number of NR iterations reaches 25; in those cases we stop the simulation.

We conclude that considerable deviations from the reference case in which $Z_n = v_n'(i_n)$ not only generally result in an increase of both the average and maximum number of NR iterations (apart from some local minima), but they also might lead to situations in which the WD NR method does not converge.

VI. Conclusions and Future Works

Theoretical and experimental results in this manuscript show that setting $Z_n = v_n'(i)$ on each one-port element at every sampling step keeps the basin of quadratic convergence of the NR method large. Experiments have also shown that the condition on the free parameters suggested by the theoretical analysis minimizes the number of iterations needed to solve a nonlinear electrical network with multiple diodes (the ring modulator circuit). In practical scenarios in which the derivative $v_n'(i_n)$ of nonlinear v–i characteristics is not available before solving the circuit at a given sampling step k, such a derivative can be estimated using the values of $v_n'(i_n)$ at the previous sampling steps, similarly to what done when applying the WD fixed-point algorithm discussed in [23], [44]–[47], [49] and called SIM.

As a future work, it is worth extending the results presented in this manuscript to circuits containing one-port nonlinearities with non-monotonic v–i characteristics and multi-port nonlinearities [24], [41], [66]. Moreover, a more general theoretical analysis aimed at investigating whether the condition $Z_n = v_n'(i)$, already known to maximize the speed of convergence of SIM [44], is the optimal port resistance choice for increasing the convergence speed and the robustness of a broader class of WD iterative methods is also left for future research.

Appendix A
Non-singularity of $\mathbf{J_g}$

By (14) and (9), $\mathbf{J_g}(\mathbf{a}) = \mathbf{S} - \mathbf{J_f}(\mathbf{a})$ is singular if and only if $\mathbf{I} - \mathbf{S}\mathbf{J_f}(\mathbf{a})$ is singular. Furthermore, (9) and (10) imply that

$$\mathbf{Z}^{-1} = \mathbf{S}^T\mathbf{Z}^{-1}\mathbf{S} \quad \Leftrightarrow \quad \mathbf{Z}^{-1}\mathbf{S} = \mathbf{S}^T\mathbf{Z}^{-1}. \tag{57}$$

Hence, the matrix $\tilde{\mathbf{S}} = \mathbf{Z}^{-\frac{1}{2}}\mathbf{S}\mathbf{Z}^{\frac{1}{2}}$ is symmetric [44]:

$$\tilde{\mathbf{S}} = \mathbf{Z}^{-\frac{1}{2}}\mathbf{S}\mathbf{Z}^{\frac{1}{2}} = \mathbf{Z}^{\frac{1}{2}}\mathbf{S}^T\mathbf{Z}^{-\frac{1}{2}} = \tilde{\mathbf{S}}^T. \tag{58}$$

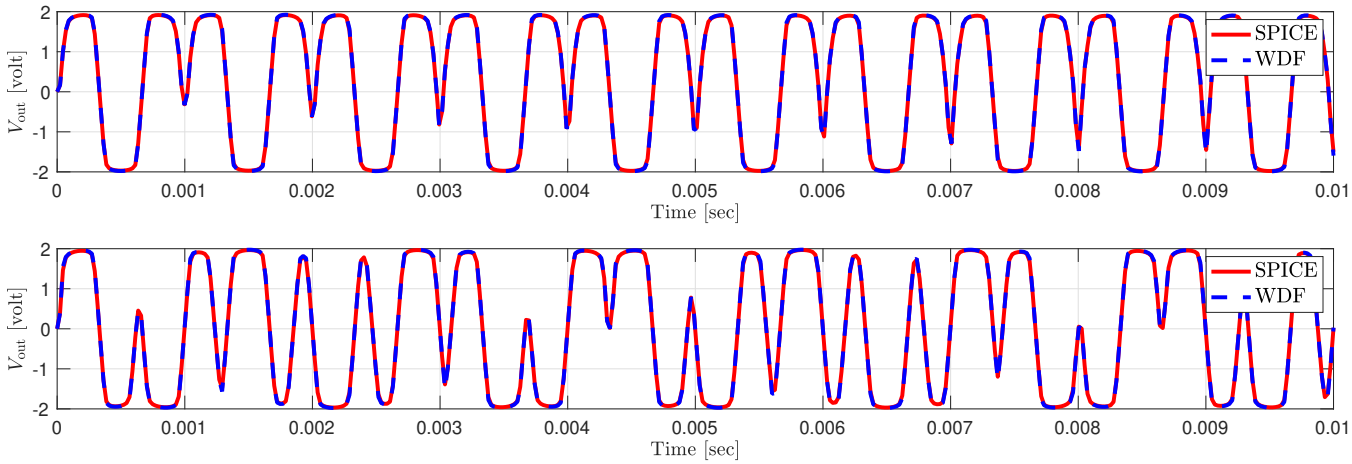

Fig. 3. Time domain simulation of the ring modulator circuit. The upper plot shows the signal V_{out} in the case in which $g_{\text{in}} = 5$ V, $f_{\text{in}} = 1500$ Hz, $g_{\text{c}} = 5$ V and $f_{\text{c}} = 500$ Hz. The lower plot shows the signal V_{out} in the case in which $g_{\text{in}} = 5$ V, $f_{\text{in}} = 1500$ Hz, $g_{\text{c}} = 5$ V and $f_{\text{c}} = 810$ Hz.

In particular from (58), $\mathbf{S}$ and $\tilde{\mathbf{S}}$ are similar and hence they have the same *spectral radius* ρ, that is the largest eigenvalue magnitude: $\rho(\mathbf{S}) = \rho(\tilde{\mathbf{S}})$. Hence, again by similarity between $\mathbf{S}\mathbf{J}_{\mathbf{f}}(\mathbf{a})$ and $\mathbf{Z}^{-1/2}\mathbf{S}\mathbf{J}_{\mathbf{f}}(\mathbf{a})\mathbf{Z}^{1/2}$, and since $\mathbf{J}_{\mathbf{f}}(\mathbf{a})$ and $\mathbf{Z}$ are both diagonal:

$$\begin{aligned}\rho\big(\mathbf{S}\mathbf{J}_{\mathbf{f}}(\mathbf{a})\big) &= \rho\big(\mathbf{Z}^{-\frac{1}{2}}\mathbf{S}\mathbf{J}_{\mathbf{f}}(\mathbf{a})\mathbf{Z}^{\frac{1}{2}}\big) = \rho\big(\tilde{\mathbf{S}}\mathbf{J}_{\mathbf{f}}(\mathbf{a})\big)\\ &\le \big\|\tilde{\mathbf{S}}\mathbf{J}_{\mathbf{f}}(\mathbf{a})\big\| \le \big\|\tilde{\mathbf{S}}\big\|\big\|\mathbf{J}_{\mathbf{f}}(\mathbf{a})\big\| \\ &= \rho\big(\tilde{\mathbf{S}}\big)\rho\big(\mathbf{J}_{\mathbf{f}}(\mathbf{a})\big) = \rho(\mathbf{S})\rho\big(\mathbf{J}_{\mathbf{f}}(\mathbf{a})\big),\end{aligned} \tag{59}$$

where we have used the matrix norm inequality $\|\mathbf{AB}\| \le \|\mathbf{A}\|\|\mathbf{B}\|$ and the inequality $\rho(\mathbf{A}) \le \|\mathbf{A}\|$, which in particular becomes an equality if $\mathbf{A}$ is symmetric and, of course, if $\mathbf{A}$ is diagonal [44], [55].

Since, by (9), all eigenvalues of $\mathbf{S}$ are equal either to 1 or -1, and by $|f(a)| < 1$, then from (59):

$$\rho\big(\mathbf{S}\mathbf{J}_{\mathbf{f}}(\mathbf{a})\big) \le \rho\big(\mathbf{S}\big)\rho\big(\mathbf{J}_{\mathbf{f}}(\mathbf{a})\big) = \rho\big(\mathbf{J}_{\mathbf{f}}(\mathbf{a})\big) < 1. \tag{60}$$

Since $\mathbf{I} - \mathbf{S}\mathbf{J}_{\mathbf{f}}(\mathbf{a})$ can be singular only if $\rho\big(\mathbf{S}\mathbf{J}_{\mathbf{f}}(\mathbf{a})\big) \ge 1$, inequality (60) implies that $\mathbf{I} - \mathbf{S}\mathbf{J}_{\mathbf{f}}(\mathbf{a})$ is non-singular.

Appendix B
An upper limit for $M(\mathbf{a})$

From (58) and (9) we have

$$\tilde{\mathbf{S}}^T\tilde{\mathbf{S}} = \tilde{\mathbf{S}}\tilde{\mathbf{S}} = \mathbf{Z}^{-\frac{1}{2}}\mathbf{S}\mathbf{S}\mathbf{Z}^{\frac{1}{2}} = \mathbf{I}. \tag{61}$$

Hence, $\tilde{\mathbf{S}}$ is orthogonal and this implies $\|\tilde{\mathbf{S}}\| = 1$.

Since $\mathbf{J}_{\mathbf{f}}(\mathbf{a})$ is diagonal, from (14), (58) and (61),

$$\begin{aligned}\mathbf{J}_{\mathbf{g}}(\mathbf{a}) &= \mathbf{Z}^{\frac{1}{2}}\tilde{\mathbf{S}}\mathbf{Z}^{-\frac{1}{2}} - \mathbf{J}_{\mathbf{f}}(\mathbf{a}) \\ &= \mathbf{Z}^{\frac{1}{2}}\big(\tilde{\mathbf{S}} - \mathbf{J}_{\mathbf{f}}(\mathbf{a})\big)\mathbf{Z}^{-\frac{1}{2}} \\ &= \mathbf{Z}^{\frac{1}{2}}\tilde{\mathbf{S}}\big(\mathbf{I} - \tilde{\mathbf{S}}\mathbf{J}_{\mathbf{f}}(\mathbf{a})\big)\mathbf{Z}^{-\frac{1}{2}}.\end{aligned} \tag{62}$$

Again making use of (61), eq. (62) can be inverted:

$$\mathbf{J}_{\mathbf{g}}^{-1}(\mathbf{a}) = \mathbf{Z}^{\frac{1}{2}}\big(\mathbf{I} - \tilde{\mathbf{S}}\mathbf{J}_{\mathbf{f}}(\mathbf{a})\big)^{-1}\tilde{\mathbf{S}}\mathbf{Z}^{-\frac{1}{2}}. \tag{63}$$

Thus, by diagonality of both $\mathbf{H}_{\mathbf{g}}(\mathbf{a})$ and $\mathbf{Z}$,

$$\mathbf{J}_{\mathbf{g}}^{-1}(\mathbf{a})\mathbf{H}_{\mathbf{g}}(\mathbf{a}) = \mathbf{Z}^{\frac{1}{2}}\big(\mathbf{I} - \tilde{\mathbf{S}}\mathbf{J}_{\mathbf{f}}(\mathbf{a})\big)^{-1}\tilde{\mathbf{S}}\mathbf{H}_{\mathbf{g}}(\mathbf{a})\mathbf{Z}^{-\frac{1}{2}}. \tag{64}$$

Since $\tilde{\mathbf{S}}$ is orthogonal, and by (59) and (60):

$$\big\|\tilde{\mathbf{S}}\mathbf{J}_{\mathbf{f}}(\mathbf{a})\big\| = \big\|\tilde{\mathbf{S}}\big\|\big\|\mathbf{J}_{\mathbf{f}}(\mathbf{a})\big\| = \big\|\mathbf{J}_{\mathbf{f}}(\mathbf{a})\big\| < 1. \tag{65}$$

Hence, $\mathbf{I} - \tilde{\mathbf{S}}\mathbf{J}_{\mathbf{f}}(\mathbf{a})$ is not singular and furthermore we can write [55]

$$\Big\|\big(\mathbf{I} - \tilde{\mathbf{S}}\mathbf{J}_{\mathbf{f}}(\mathbf{a})\big)^{-1}\Big\| \le \frac{1}{1 - \big\|\tilde{\mathbf{S}}\mathbf{J}_{\mathbf{f}}(\mathbf{a})\big\|}. \tag{66}$$

Then, finally from (64), (66), and (65):

$$\begin{aligned}&\big\|\mathbf{J}_{\mathbf{g}}^{-1}(\mathbf{a})\mathbf{H}_{\mathbf{g}}(\mathbf{a})\big\| \\ &\quad= \big\|\mathbf{Z}^{\frac{1}{2}}\big\|\Big\|\big(\mathbf{I} - \tilde{\mathbf{S}}\mathbf{J}_{\mathbf{f}}(\mathbf{a})\big)^{-1}\tilde{\mathbf{S}}\mathbf{H}_{\mathbf{g}}(\mathbf{a})\Big\|\big\|\mathbf{Z}^{-\frac{1}{2}}\big\| \\ &\quad= \sqrt{\frac{Z_{\max}}{Z_{\min}}}\,\Big\|\big(\mathbf{I} - \tilde{\mathbf{S}}\mathbf{J}_{\mathbf{f}}(\mathbf{a})\big)^{-1}\tilde{\mathbf{S}}\mathbf{H}_{\mathbf{g}}(\mathbf{a})\Big\| \\ &\quad\le \sqrt{\frac{Z_{\max}}{Z_{\min}}}\,\Big\|\big(\mathbf{I} - \tilde{\mathbf{S}}\mathbf{J}_{\mathbf{f}}(\mathbf{a})\big)^{-1}\Big\|\big\|\tilde{\mathbf{S}}\mathbf{H}_{\mathbf{g}}(\mathbf{a})\big\| \\ &\quad\le \sqrt{\frac{Z_{\max}}{Z_{\min}}}\,\frac{\big\|\tilde{\mathbf{S}}\mathbf{H}_{\mathbf{g}}(\mathbf{a})\big\|}{1 - \big\|\tilde{\mathbf{S}}\mathbf{J}_{\mathbf{f}}(\mathbf{a})\big\|} = \sqrt{\frac{Z_{\max}}{Z_{\min}}}\,\frac{\big\|\mathbf{H}_{\mathbf{g}}(\mathbf{a})\big\|}{1 - \big\|\mathbf{J}_{\mathbf{f}}(\mathbf{a})\big\|}.\end{aligned} \tag{67}$$

This inequality proves (30) and, as a particular case, (29).

References

[1] D. T.-M. Yeh, "Digital implementation of musical distortion circuits by analysis and simulation," Ph.D. diss., Stanford Univ., CA, June 2009.
[2] G. De Sanctis and A. Sarti, "Virtual analog modeling in the wave-digital domain," *IEEE Trans. Audio, Speech, Language Process.*, vol. 18, pp. 715–727, May 2010.
[3] V. Välimäki, S. Bilbao, J. O. Smith, J. S. Abel, J. Pakarinen, and D. Berners, *Virtual Analog Effects*, 2nd ed. John Wiley & Sons, Ed. Udo Zölzer, 2011, ch. 12, pp. 473–522.
[4] S. D'Angelo, "Virtual analog modeling of nonlinear musical circuits," Ph.D. Dissertation, Aalto University, Espoo, Finland, Sept. 2014.
[5] K. J. Werner, "Virtual analog modeling of audio circuitry using wave digital filters," Ph.D. diss., Stanford Univ., CA, Dec. 2016, [Online at https://searchworks.stanford.edu/view/11891203; accessed 1-July-2019].
[6] S. D'Angelo, "Lightweight virtual analog modeling," in *Proc. XXII Colloquio di Informatica Musicale (CIM)*, Udine, Italy, Nov. 2018.
[7] A. Bernardini and A. Sarti, "Towards inverse virtual analog modeling," in *Proc. 22nd Int. Conf. Digital Audio Effects*, Birmingham, UK, Sept. 2–6 2019.
[8] E. Barbour, "The cool sound of tubes [vacuum tube musical applications]," *IEEE Spectrum*, vol. 35, no. 8, pp. 24–35, 1998.

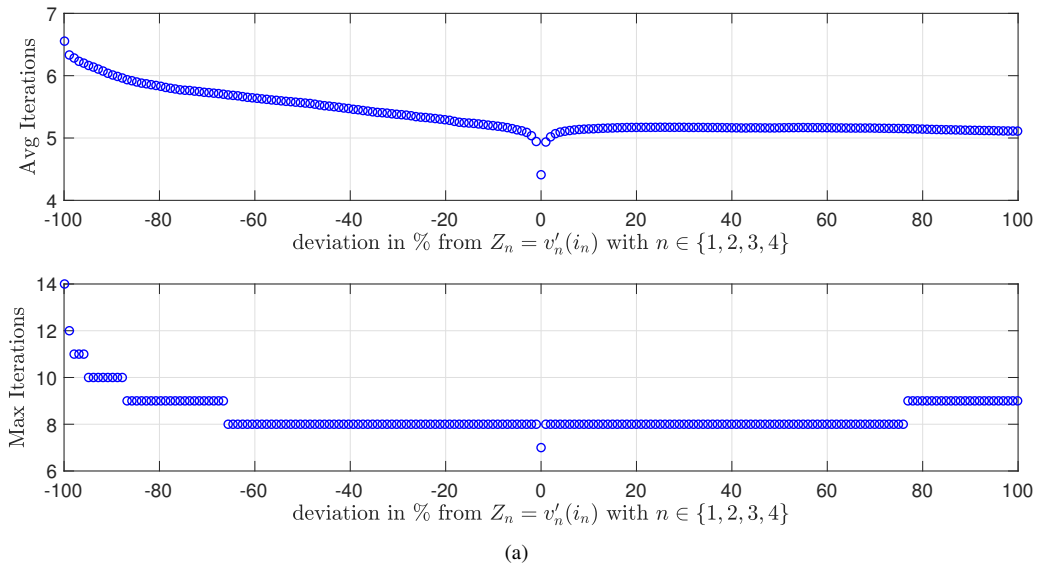

(a)

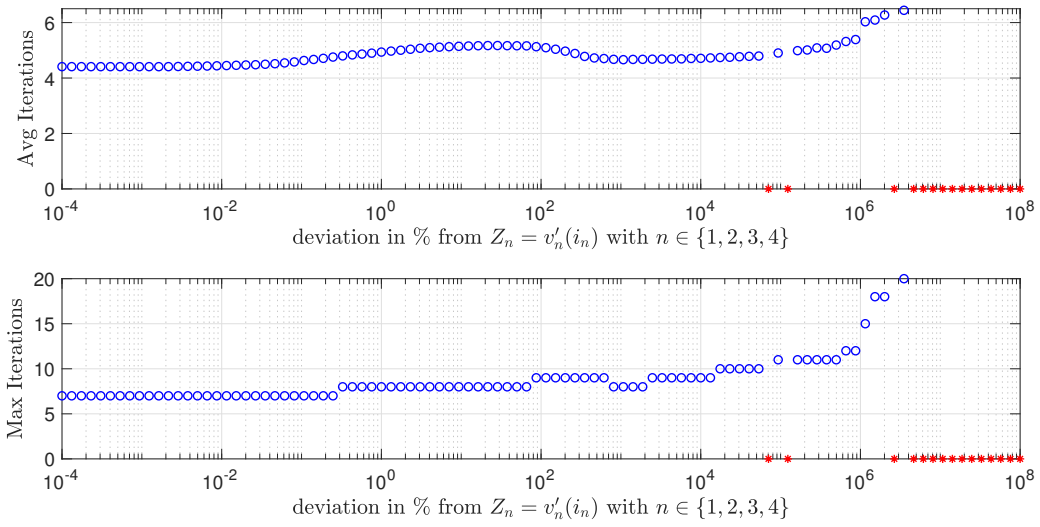

(b)

Fig. 4. In both subfigures (each one containing a pair of plots), blue circles represent the average number of NR iterations (upper plot) and the maximum number of NR iterations (lower plot) for different settings of the free parameters $Z_1, \ldots, Z_4$. On the x-axis we have the deviation in percentage with respect to the reference setting in which $Z_n = v'_n(i_n)$. Different ranges of deviation are considered in the two subfigures. Fig. 4(a) shows the result of 200 simulations in the deviation range $[-99.9\%, 99.9\%]$ represented in linear scale. Fig. 4(b) shows the result of 100 simulations in the deviation range $[10^{-4}\%, 10^{8}\%]$ represented in log scale. The red asterisks on the x-axis in Fig. 4(b) refer to simulations in which the number of NR iterations reaches 25; in those cases we stop the simulation.

[9] T. Helie, "Volterra series and state transformation for real-time simulations of audio circuits including saturations: Application to the moog ladder filter," *IEEE Trans. on Audio, Speech, and Language Processing*, vol. 18, no. 4, pp. 747–759, May 2010.

[10] F. Eichas and U. Zölzer, "Gray-box modeling of guitar amplifiers," *J. Audio Eng. Soc*, vol. 66, no. 12, pp. 1006–1015, 2018.

[11] A. Novak, L. Simon, F. Kadlec, and P. Lotton, "Nonlinear system identification using exponential swept-sine signal," *IEEE Trans. Instrum. Meas.*, vol. 59, no. 8, pp. 2220–2229, Aug 2010.

[12] T. Schmitz and J. J. Embrechts, "Nonlinear real-time emulation of a tube amplifier with a long short time memory neural-network," in *Audio Engineering Society Convention 144*, May 2018.

[13] E. Damskagg, L. Juvela, E. Thuillier, and V. Välimäki, "Deep learning for tube amplifier emulation," in *ICASSP 2019 - 2019 IEEE International Conference on Acoustics, Speech and Signal Processing (ICASSP)*, 2019, pp. 471–475.

[14] A. Carini, S. Cecchi, M. Gasparini, and G. L. Sicuranza, "Introducing legendre nonlinear filters," in *IEEE Int. Conf. on Acoustics, Speech and Signal Processing (ICASSP)*, May 2014, pp. 7939–7943.

[15] D. T. Yeh, J. S. Abel, and J. O. Smith, "Automated physical modeling of nonlinear audio circuits for real-time audio effects - part 1: Theoretical development," *IEEE Trans. Audio, Speech, Language Process.*, vol. 18, pp. 728–737, May 2010.

[16] K. Dempwolf, M. Holters, and U. Zölzer, "Discretization of parametric analog circuits for real-time simulations," in *Proc. 13th Conf. Digital Audio Effects*, Graz, Austria, Sept. 42–49 2010.

[17] A. Falaize and T. Hélie, "Passive guaranteed simulation of analog audio circuits: A port-Hamiltonian approach," *Applied Sciences*, vol. 6, no. 10, 2016.

[18] A. Fettweis, "Wave digital filters: Theory and practice," *Proc. IEEE*, vol. 74, no. 2, pp. 270–327, Feb. 1986.

[19] R. C. D. Paiva, S. D'Angelo, J. Pakarinen, and V. Välimäki, "Emulation of operational amplifiers and diodes in audio distortion circuits," *IEEE Trans. Circuits Syst. II, Exp. Briefs*, vol. 59, pp. 688–692, Oct. 2012.

[20] S. D'Angelo, J. Pakarinen, and V. Välimäki, "New family of wave-digital triode models," *IEEE Trans. Audio, Speech, Language Process.*, vol. 21, pp. 313–321, Feb. 2013.

[21] M. Verasani, A. Bernardini, and A. Sarti, "Modeling Sallen-Key audio

filters in the wave digital domain," in *2017 IEEE International Conference on Acoustics, Speech and Signal Processing (ICASSP)*, March 2017, pp. 431–435.

[22] K. J. Werner, A. Bernardini, J. O. Smith, and A. Sarti, "Modeling circuits with arbitrary topologies and active linear multiports using wave digital filters," *IEEE Transactions on Circuits and Systems I: Regular Papers*, vol. 65, no. 12, pp. 4233–4246, Dec. 2018.

[23] A. Bernardini, P. Maffezzoni, and A. Sarti, "Linear multistep discretization methods with variable step-size in nonlinear wave digital structures for virtual analog modeling," *IEEE/ACM Transactions on Audio, Speech, and Language Processing*, vol. 27, no. 11, pp. 1763–1776, Nov. 2019.

[24] A. Bernardini, A. E. Vergani, and A. Sarti, "Wave digital modeling of nonlinear 3-terminal devices for virtual analog applications," *Circuits, Systems, and Signal Processing*, vol. 39, pp. 3289–3319, Jan. 2020.

[25] F. Pedersini, A. Sarti, and S. Tubaro, "Object-based sound synthesis for virtual environments using musical acoustics," *IEEE Signal Process. Mag.*, vol. 17, no. 6, pp. 37–51, Nov. 2000.

[26] R. Rabenstein, S. Petrausch, A. Sarti, G. D. Sanctis, C. Erkut, and M. Karjalainen, "Blocked-based physical modeling for digital sound synthesis," *IEEE Signal Processing Magazine*, vol. 24, no. 2, pp. 42–54, March 2007.

[27] G. Borin, G. De Poli, and D. Rocchesso, "Elimination of delay-free loops in discrete-time models of nonlinear acoustic systems," *IEEE Trans. Acoust., Speech, Signal Process.*, vol. 8, pp. 597–605, Sept. 2000.

[28] K. Meerkötter and R. Scholz, "Digital simulation of nonlinear circuits by wave digital filter principles," in *IEEE Int. Symp. Circuits Syst.*, May 8–11 1989, pp. 720–723.

[29] A. Sarti and G. De Sanctis, "Systematic methods for the implementation of nonlinear wave-digital structures," *IEEE Trans. Circuits Syst. I, Reg. Papers*, vol. 56, pp. 460–472, Feb. 2009.

[30] A. Bernardini, K. J. Werner, A. Sarti, and J. O. Smith, "Modeling a class of multi-port nonlinearities in wave digital structures," in *Proc. 23rd European Signal Processing Conference (EUSIPCO)*, Nice, France, Aug. 31 – Sept. 4 2015, pp. 669–673.

[31] A. Bernardini and A. Sarti, "Dynamic adaptation of instantaneous nonlinear bipoles in wave digital networks," in *Proc. 24th European Signal Processing Conference (EUSIPCO)*, Budapest, Hungary, Aug. 29 – Sept. 2 2016, pp. 1038–1042.

[32] A. Bernardini, K. J. Werner, A. Sarti, and J. O. Smith III, "Modeling nonlinear wave digital elements using the Lambert function," *IEEE Transactions on Circuits and Systems I: Regular Papers*, vol. 63, no. 8, pp. 1231–1242, Aug. 2016.

[33] A. Bernardini and A. Sarti, "Canonical piecewise-linear representation of curves in the wave digital domain," in *Proc. 25th European Signal Processing Conference (EUSIPCO)*, Aug 2017, pp. 1125–1129.

[34] D. Albertini, A. Bernardini, and A. Sarti, "Antiderivative antialiasing techniques in nonlinear wave digital structures," *accepted for publication in Journal of the Audio Engineering Society*, 2021, https://doi.org/10.17743/jaes.2021.0017.

[35] C. W. Ho, A. E. Ruehli, and P. A. Brennan, "The modified nodal approach to network analysis," *IEEE Trans. Circuits Syst.*, vol. 22, no. 6, pp. 504–509, June 1975.

[36] M. Holters and U. Zölzer, "Physical modeling of a wah-wah effect pedal as a case study for application of the nodal dk method to circuits with variable parts," in *Proc. 14th Conf. Digital Audio Effects*, Paris, France, Sept. 19–23 2011.

[37] A. Bernardini and A. Sarti, "Biparametric wave digital filters," *IEEE Transactions on Circuits and Systems I: Regular Papers*, vol. 64, no. 7, pp. 1826–1838, July 2017.

[38] C. Christoffersen, "Transient analysis of nonlinear circuits based on waves," in *Scientific Computing in Electrical Engineering SCEE 2008*, L. R. Costa and J. Roos, Eds. Berlin Heidelberg: Springer Verlag, 2010, pp. 159–166.

[39] M. Kabir, C. Christoffersen, and N. Kriplani, "Transient simulation based on state variables and waves," *International Journal of RF and Microwave Computer-Aided Engineering*, vol. 21, no. 3, pp. 314–324, 2011.

[40] T. Schwerdtfeger and A. Kummert, "A multidimensional approach to wave digital filters with multiple nonlinearities," in *22nd Proc. European Signal Process. Conf.*, Lisbon, Portugal, Sept. 1–5 2014, pp. 2405–2409.

[41] T. Schwerdtfeger and A. Kummert, "Nonlinear circuit simulation by means of Alfred Fettweis' wave digital principles," *IEEE Circuits and Systems Magazine*, vol. 19, no. 1, pp. 55–C3, Firstquarter 2019.

[42] T. Schwerdtfeger and A. Kummert, "Newton's method for modularity-preserving multidimensional wave digital filters," in *Proc. IEEE Int. Work. Multidimensional Syst.*, Vila Real, Portugal, Sept. 2015.

[43] M. J. Olsen, K. J. Werner, and J. O. Smith III, "Resolving grouped nonlinearities in wave digital filters using iterative techniques," in *Proc. 19th Int. Conf. Digital Audio Effects*, Brno, Czech Republic, Sept. 2016, pp. 279–286.

[44] A. Bernardini, P. Maffezzoni, L. Daniel, and A. Sarti, "Wave-based analysis of large nonlinear photovoltaic arrays," *IEEE Trans. Circuits Syst. I, Reg. Papers*, vol. 65, no. 4, pp. 1363–1376, Apr. 2018.

[45] A. Bernardini, A. Sarti, P. Maffezzoni, and L. Daniel, "Wave digital-based variability analysis of electrical mismatch in photovoltaic arrays," in *Proc. IEEE Int. Symp. Circuits Syst. (ISCAS)*, May 2018, pp. 1–5.

[46] A. Bernardini, K. J. Werner, P. Maffezzoni, and A. Sarti, "Wave digital modeling of the diode-based ring modulator," in *Proc. 144th Audio Eng. Soc. Conv.*, Milan, Italy, May 24–26 2018, conv. paper #10015.

[47] A. Proverbio, A. Bernardini, and A. Sarti, "Toward the Wave Digital Real-Time Emulation of Audio Circuits with Multiple Nonlinearities," in *2020 28th European Signal Processing Conference (EUSIPCO)*, Amsterdam, The Netherlands, 2021, pp. 151–155.

[48] R. Giampiccolo, A. Bernardini, G. Gruosso, P. Maffezzoni, and A. Sarti, "Multiphysics Modeling of Audio Circuits with Nonlinear Transformers," *Journal of the Audio Engineering Society*, vol. 69, no. 6, June 2021, https://doi.org/10.17743/jaes.2021.0008.

[49] D. Albertini, A. Bernardini, and A. Sarti, "Scattering Iterative Method based on generalized wave variables for the implementation of audio circuits with multiple one-port nonlinearities," in *Proc. 150th Convention of the Audio Engineering Society*, Online, May 25–28 2021.

[50] A. Fettweis and G. Nitsche, "Numerical integration of partial differential equations by means of multidimensional wave digital filters," in *Proc. IEEE Int. Symp. Circuits Syst.*, New Orleans, LA, May 1990, pp. 954–957.

[51] L. Kolonko, J. Velten, and A. Kummert, "Automatic differentiating wave digital filters with multiple nonlinearities," in *2020 28th European Signal Processing Conference (EUSIPCO)*, Amsterdam, The Netherlands, 2021, pp. 146–150.

[52] F. Fontana and E. Bozzo, "Newton-Raphson solution of nonlinear delay-free loop filter networks," *IEEE/ACM Transactions on Audio, Speech, and Language Processing*, vol. 27, no. 10, pp. 1590–1600, 2019.

[53] K. Atkinson, *An Introduction to Numerical Analysis*. Wiley, 1989.

[54] A. Bernardini, K. J. Werner, J. O. Smith, and A. Sarti, "Generalized wave digital filter realizations of arbitrary reciprocal connection networks," *IEEE Transactions on Circuits and Systems I: Regular Papers*, vol. 66, no. 2, pp. 694–707, Feb. 2019.

[55] R. A. Horn and C. R. Johnson, *Matrix Analysis*, 2nd ed. NY, USA: Cambridge University Press, 2012.

[56] K. J. Werner, V. Nangia, A. Bernardini, J. O. Smith, and A. Sarti, "An improved and generalized diode clipper model for wave digital filters," in *Proc. Conv. Audio Eng. Soc.*, New York, NY, Oct. 29 – Nov. 1 2015.

[57] S. D'Angelo, L. Gabrielli, and L. Turchet, "Fast approximation of the lambert w function for virtual analog modelling," in *Proc. 22nd Int. Conf. Digital Audio Effects (DAFx)*, Birmingham, UK, September 2–6 2019.

[58] F. A. Cowan, "Modulating system," USA Patent 2,025,158, June 24, 1935, U.S. Patent # 2,025,158, Filed 7 June 1934, Issued 24 Dec. 1935.

[59] H. Bode, "History of electronic sound modification," *J. Audio Eng. Soc.*, vol. 32, no. 10, pp. 730–739, Oct 1984.

[60] J. Parker, "A simple digital model of the diode-based ring-modulator," in *Proc. Int. Conf. Digital Audio Effects*, Paris, France, Sept. 19–23 2011, pp. 163–166.

[61] T. E. Oberheim, "A "ring modulator" device for the performing musician," in *Proc. Audio Eng. Soc. 38th Conv.*, May 4–7 1970.

[62] R. Hoffmann-Burchardi, "Digital simulation of the diode ring modulator for musical applications," in *Proc. 11th Int. Conf. Digital Audio Effects*, Espoo, Finland, September 1–4 2008, pp. 165–168.

[63] ——, "Asymmetries make the difference: An analysis of transistor-based analog ring modulators," in *Proc. 12th Int. Conf. Digital Audio Effects*, Como, Italy, September 1–4 2009.

[64] G. O. Martens and K. Meerkötter, "On N-port adaptors for wave digital filters with application to a bridged-tee filter," in *Proc. IEEE Int. Symp. Circuits Syst.*, Munich, Germany, Apr. 1976, pp. 514–517.

[65] S. D'Angelo, L. Gabrielli, and L. Turchet, "Fast approximation of the Lambert W function for virtual analog modelling," in *Proc. 22nd Int. Conf. Digital Audio Effects*, Birmingham, UK, September 2–6 2019.

[66] A. Bernardini, P. Maffezzoni, and A. Sarti, "Vector wave digital filters and their application to circuits with two-port elements," *IEEE Transactions on Circuits and Systems I: Regular Papers*, vol. 68, no. 3, pp. 1269–1282, 2021.

Alberto Bernardini (S'16–M'19) received his B.S. degree from the University of Bologna, Italy, in 2012 and his M.S. degree (cum laude) from the Politecnico di Milano, Italy, in 2015, both in Computer Engineering. In 2019, he received his Ph.D. degree (cum laude) in Information Engineering from the Politecnico di Milano, where he is currently a post-doctoral researcher. His main research interests are audio signal processing and modeling of nonlinear systems. He authored over 20 publications in international journals and proceedings of international conferences. He is also the first author of an international patent.

Enrico Bozzo received the Laurea degree in computer science from the University of Udine, Italy, in 1990 and the Ph.D. degree in computer science from the University of Pisa, Italy, in 1994. He is currently an Assistant Professor in the Department of Mathematics, Computer Science and Physics, University of Udine, teaching numerical analysis. He was a team member in several national research projects. His current interests are in numerical linear algebra, in particular matrix theory and its applications.

Federico Fontana (SM'11) received the Laurea degree in electronic engineering from the University of Padova, Italy, in 1996 and the Ph.D. degree in computer science from the University of Verona, Italy, in 2003. During the Ph.D. degree studies, he was a Research Consultant in the design and realization of real-time audio DSP systems. He is currently an Associate Professor in the Department of Mathematics, Computer Science and Physics, University of Udine, Italy, teaching Auditory & tactile interaction and Computer architectures. In 2001, he was Visiting Scholar at the Laboratory of Acoustics and Audio Signal Processing, Helsinki University of Technology, Espoo, Finland. His current interests are in interactive sound processing methods and in the design and evaluation of musical interfaces. Professor Fontana coordinated the EU project 222107 NIW under the FP7 ICT-2007.8.0 FET-Open call from 2008 to 2011. From 2017 to 2021, he served as Associate Editor of the IEEE/ACM TRANSACTIONS ON AUDIO, SPEECH, AND LANGUAGE PROCESSING.

Augusto Sarti (M'04–SM'13) received his Ph.D. in Information Engineering from the University of Padova, Italy, in 1993, with a joint graduate program with the University of California, Berkeley. In 1993, he joined the Politecnico di Milano (PoliMI), Italy, where he is currently a Full Professor. From 2013 to 2017 he held a professorship at the University of California, Davis. At PoliMI he currently coordinates the research activities of the Musical Acoustics Lab and the Sound and Music Computing Lab, and the M.Sci. program in "Music and Acoustic Engineering". He has coauthored over 300 scientific publications on international journals and congresses and numerous patents in the multimedia signal processing area. His current research interests are in the area of audio and acoustic signal processing, with particular focus on spatial audio signal processing; music information retrieval; and musical acoustics. He served two terms with the IEEE Technical Committee on Audio and Acoustics Signal Processing. He also served as Associate Editor of IEEE/ACM Tr. on Audio Speech and Language Processing, and as Senior Area Editor of IEEE Signal Processing Letters. He is currently serving in the EURASIP board of directors.